Characterization and anticancer bioactivity of the fungal immunomodulatory protein FIP-Gre from Ganoderma resinaceum

RUBAB AMEEN AMEEN
University of the Punjab
ALEENA SUMRIN SUMRIN
aleena.camb@pu.edu.pk
University of the Punjab

Research Article

Keywords: Ganoderma resinaceum, FIP-Gre, Fungal Immunomodulatory Proteins, EGFR, c-Met, A549 lung adenocarcinoma, apoptosis

Posted Date: January 6th, 2026

DOI: https://doi.org/10.21203/rs.3.rs-8423392/v1

Additional Declarations: No competing interests reported.

Abstract

Background: Natural products remain rich sources of anticancer agents. Fungal immunomodulatory proteins (FIPs) from medicinal mushrooms show direct in vitro tumor inhibition; we investigated a new FIP, FIP-Gre, from *Ganoderma resinaceum*.

Methods: FIP-Gre was identified by genome mining (LZ8 query), modeled by AlphaFold2, and assessed by docking/100-ns MD (EGFR, c-Met). Recombinant FIP-Gre was produced in E. coli BL21 (DE3)/pET-29a (+), purified by Ni-NTA (~12.5 kDa), and tested for hemagglutination, antibacterial activity, cytotoxicity (A549, HepG2, MCF-7; HEK-293 control), and apoptosis markers in A549 cells (8 µg/mL).

Results:FIP-Gre shares 90% identity with LZ8, contains a conserved Fve-type domain, and adopts a stable β-strand–rich fold. Docking/MD suggest strong, stable binding to EGFR and c-Met. FIP-Gre agglutinated mouse RBCs at 4 µg/mL, showed no antibacterial activity, and selectively inhibited cancer cells with **IC_{50} values of 21.27µg/mL (A549), 29.96µg/mL (HepG2), and 43.34µg/mL (MCF-7)** while showing no toxicity toward normal HEK-293 cells. At 8 µg/mL, FIP-Gre significantly induced apoptosis in A549 cells by **upregulating Bax, Caspase-3, Caspase-9, and p53,** and **downregulating Bcl-2**, indicating activation of the mitochondrial apoptotic pathway.

Conclusion: FIP-Gre is a structurally robust, mushroom-derived protein with selective in vitro anticancer activity and predicted RTK engagement, supporting its development, particularly against lung carcinoma.

Introduction

Common edible and medicinal mushrooms like *Ganoderma lucidum* (also called LZ-8 or FIP-Glu) contain a novel class of bioactive proteins called FIPs, *V. volvacea* (also known as FIP-vvo) [1], *F. velutipes (*also known as FIP-fve) [2] [2]and *G. sinensis* (also known as FIP-gsi) [3]. FIPs attracted scientific interest ever since their discovery due to their bioactive properties including hemagglutination and anti-inflammation and immunomodulation and anti-cancer effects [4]. Research shows that Fungal immunomodulatory proteins (FIPs) behave as critical bioactive compounds which exhibit potential benefits against cancer. The mechanisms of action for these proteins include triggering natural cell death and stopping cells from reproducing along with altering immune system response and more. The inhibitory activity of LZ-8 produced by *Ganoderma lucidum* has been confirmed through its ability to stop A549 lung cancer cell growth by targeting epidermal growth factor receptor (EGFR) destruction. FIP-fve from *Flammulina velutipes* lowers RacGAP1 expression to decrease Rac1 activity preventing A549 cell invasion. The anti-tumor effect of FIP-nha derived from *Nectria haematococca* against gastric cancer cells manifests through its binding to EGFR receptors which stop the EGFR-mediated signal transmission from STAT3 to Akt leading to cancer cell autophagy and apoptosis at multiple targets.

The biological activity of fungal immunomodulatory proteins (FIPs) is primarily attributed to conserved structural features, particularly their homodimerization capability. Advances in genome sequencing have accelerated the identification of novel FIPs with anticancer and immunomodulatory potential. Studies on *Ganoderma lucidum*–derived FIPs have provided important insights into their structure–function relationships and therapeutic relevance [5]. Since their first discovery in 1989, approximately thirty FIPs have been identified, forming a distinct protein family characterized by shared sequence and structural features [6].Functionally, FIPs exert antitumor effects through a combination of direct cytotoxicity and immune modulation, supporting their potential as candidates for anticancer applications.

Angiogenesis, cell migration, and proliferation are regulated by growth factor receptors, particularly receptor tyrosine kinases (RTKs), which control key cellular processes including survival, division, and apoptosis [7]. Epidermal growth factor receptor (EGFR), a 170-kDa transmembrane glycoprotein of the ErbB family, undergoes ligand-induced dimerization and autophosphorylation, activating downstream signaling pathways such as PI3K/Akt, JAK/STAT, and Ras/Raf that promote tumor growth, invasion, and metastasis [8]. EGFR is frequently overexpressed in epithelial malignancies, making it an established therapeutic target. Clinically approved EGFR tyrosine kinase inhibitors, including erlotinib and gefitinib, enhance the efficacy of chemotherapy and radiotherapy by blocking oncogenic signaling and inducing apoptosis [9]. Hepatocyte growth factor signals through the c-Met receptor to regulate cell proliferation, motility, and morphogenesis, and aberrant activation of both EGFR and c-Met through mutation or amplification contributes to cancer progression, highlighting their importance as targets for anticancer intervention [10].

In this study, we present FIP-Gre, a novel fungal immunomodulatory protein discovered through genome mining of *Ganoderma resinaceum*, as a potential inhibitor for cancer therapy. Phylogenetic and sequence analyses reveal its close evolutionary relationship with FIP-Glu (LZ8) and other fungal immunomodulatory proteins (FIPs), suggesting that FIP-Gre may share similar biological activities. Structural modeling, validated through AlphaFold2, confirms its potential for functional studies. It has been demonstrated by Molecular docking and molecular dynamics simulations studies that FIP-Gre binds stably to key receptor tyrosine kinases, EGFR and c-Met, which are critical regulators of cancer progression, pointing to its ability to disrupt oncogenic signaling pathways. These findings establish FIP-Gre as a promising candidate for targeted cancer therapies, particularly in inhibiting receptor tyrosine kinase-driven malignancies. To validate these findings experimentally, FIP-

Gre was cloned, expressed in *E. coli*, and purified for functional studies. In vitro assays demonstrated hemagglutination, antimicrobial activity, and dose-dependent cytotoxicity against cancer cell lines, confirming its anticancer potential.

Materials

The bacterial cultures used in the present study were obtained from stock culture of Department of Microbiology and Molecular Genetics (MMG), University of the Punjab. Bacterial strains used were *E. coli, Klebsiella pneumoniae, Staphylococcus aureus, Pseudomonas aeruginosa and Salmonella typhi.* The cancer cell lines used in this study were obtained from MMG and Centre for Excellence in Molecular Biology department (CEMB), Punjab University Lahore.

Methods:

Genome Mining and Bioinformatics analysis:

A novel fungal immunomodulatory protein (FIP), designated FIP-Gre, was identified from the genome of *Ganoderma resinaceum*. FIP-Glu (LZ8) from *G. lucidum* (GenBank accession: P14945.2) was retrieved from NCBI (https://www.ncbi.nlm.nih.gov/) and used as a BLASTp query to identify homologous sequences[11]. The physiochemical properties of FIP-Gre were predicted by using ProtParam web tool (https://web.expasy.org/protparam/)[12]. The hydrophilicity of FIP-Gre was predicted by ProtScale tool (https://web.expasy.org/protscale/). Conserved domain annotation was performed using the InterPro server (https://www.ebi.ac.uk/interpro/) [13]. Protein sequences of related FIPs obtained from NCBI were aligned using ClustalX, and phylogenetic analysis was conducted with MEGA v7.0 (https://www.megasoftware.net) [14] employing the neighbor joining method with 1,000 bootstrap replicates to assess branch support [15]. The secondary structure of FIP-Gre was predicted by NPS tool (https://npsa.lyon.inserm.fr/cgi-bin/npsa_automat.pl?page=/NPSA/npsa_sopma.html). The 3D structure of FIP-Gre was modeled using trRosetta, AlphaFold2, and I-TASSER and evaluated with PROCHECK by SAVESv6.1[16]. The reference proteins 3D structures, FIP-Glu (3F3H), EGFR (3P0Y) and C-met (2uzx) were retrieved from the Protein Databank (PDB) https://www.rcsb.org/.

Protein Docking and Molecular Dynamic Simulations:

Interaction interfaces of receptors and proteins were predicted using the HADDOCK server. Focused docking was performed with the ZDOCK server [17] and the top-ranked complexes were visualized in PyMOL and analyzed with PDBsum [18]. The most stable docked complexes of FIP-Gre and FIP-Glu with EGFR and c-Met were subjected to 100-ns molecular dynamics (MD) simulations using the GROMACS package. RMSD, RMSF and hydrogen bonding were analyzed under standard conditions to assess stability [19].

Cloning, Expression and Purification of rFIPs:

After codon optimization for E. coli, the genes encoding FIP-Glu (LZ8) and FIP-Gre were synthesized (Molecular Biology Products, Pakistan) and cloned into the pET-29a(+) vector. After being verified by agarose gel electrophoresis and double digestion, the recombinant plasmids were subsequently transformed into E. coli Top10F' cells. Using colony PCR, positive transformants were found, and plasmid DNA was recovered and confirmed by PCR using forward and reverse primers including LZ8F(NdeI)5’TCTGACACGGCATTAATATTTC3’,LZ8R(XhoI)5’GTTCCACTGTGCTATTATGAAGTC3’,FIPGreF(NdeI)5’AGCTCGCATAACGACTCC3’and FIPGreR(XhoI)5’GTTCCATTGGGCTATCAGG3’.

For expression, the verified constructs were transferred into *E. coli* BL21(DE3). IPTG was used to induce protein expression at the concentrations of 0.1, 0.5, and 1.0 mM with maximal expression observed at 0.5 mM. The predicted molecular weights of rFIP-Glu and rFIP-Gre were represented by separate protein bands in SDS-PAGE analysis. These were then confirmed by Western blot with anti-His antibodies. The Bradford assay was used to measure the yields after proteins were purified using Ni-NTA affinity chromatography at ideal pH levels.

Evaluation of Hemagglutination Activity of rFIPs:

A volume of 25–100 µL of extract and a concentration of 5% of RBCs solution were required by the micro assay. A microtiter plate with U-bottomed wells was used to perform the assay. An equal volume of 50 µL of FIP-LZ8 and FIP-Gre was added to i.e. well 3 of each row. Subsequently, serial dilutions were made up to well 12 (128, 64, 32, 16, 8, 4, 2, 1, 0.5, 0.25µg/ml). The 1st well of each row was for the negative control (25 µL 1× PBS and 25 µL of a 5% suspension of red blood cells) and the 2nd well of each row was for the positive control (Phytohaemagglutinin or PHA 2µg/mL). The mixture was incubated at room temperature for 1 hour. The results are recorded.

Evaluation of antibacterial activity by agar well diffusion assay:

The agar diffusion method was used to evaluate the susceptibility of bacteria for rLZ8 and rFIP-Gre [20]. The reference strains were grown overnight and adjusted to a 1 × 10^8 CFU/mL). 5 mm wells were punched into LB agar plates and then inoculated with 100 µL of rFIPs at different concentrations of 25µg/ml, 50µg/ml and 100µg/ml. The standard antibiotics were used as positive control including Nitrofurantoin (300 ug), Linezolid 30ug) Ceftriaxone (30ug) and Colistin (10ug) against *E. coli, Staphylococcus aureus, Salmonella typhi, Pseudomonas aeruginosa and Klebsiella pneumoniae* respectively. Protein storage buffer was used as negative control. The zones of inhibition were measured after incubation as a function for bacterial susceptibility.

Evaluation of Cytotoxic Activity:

Human cancer cell lines HepG2 (hepatocellular carcinoma), MCF-7 (breast carcinoma), A549 (lung adenocarcinoma), and non-cancerous HEK-293 (embryonic kidney) were cultured at 37 °C, 5% CO_2 in DMEM supplemented with 10% FBS, 100 U/mL penicillin, and 100 µg/mL streptomycin [21]. The cells were counted using the hemocytometer [22] and seeded into 96-well plates at 1 × 10^4 cells/well in 100 µL medium and incubated for 24 h at 37 ˚C.

Cell Viability Assay:

Cell viability was evaluated using the MTT assay (Millipore Corp., Billerica, MA). Cells were treated with recombinant fungal immunomodulatory proteins at concentrations of 1–64 µg/mL for 24 h at 37 °C in 5% CO_2 (n = 3). Culture medium was replaced with fresh medium, followed by addition of MTT solution (10 µL, 5 mg/mL) and incubation for 4 h. Formazan crystals were dissolved in dimethyl sulfoxide (100 µL), and absorbance was measured at 570 nm with a reference wavelength of 630 nm using a microplate reader. Cell viability was calculated relative to untreated controls [23].

Anti-Cancer Activity Assay:

Gene Expression Studies:

Expression of apoptosis-related genes (BAX, BCL2, TP53, CASP3, and CASP9) was analyzed by RT-qPCR using GAPDH as an internal control. A549 cells were seeded in 12-well plates (2 × 10^6 cells/well) and treated with recombinant FIPs (8 µg/mL) for 24 h; control cells received PBS with medium. Total RNA was extracted using TRIzol [24], quantified by NanoDrop, and reverse-transcribed using the RevertAid First Strand cDNA Synthesis Kit (Thermo Scientific, K1612). qPCR was performed on a PikoReal™ system using SYBR Green chemistry and gene-specific primers (Supplementary Table 1). Relative expression was calculated using the ΔΔCt method after 35 cycles and normalized to GAPDH.

Statistical Analysis:

All experiments were performed in triplicate and repeated independently at least three times. Data are expressed as mean ± standard deviation (SD). Statistical analysis was conducted using one-way ANOVA in GraphPad Prism v8.0, with $p < 0.05$ considered statistically significant.

Results

Genome mining and Bioinformatics analysis:

A previously uncharacterized protein was found in the genome of *Ganoderma resinaceum* using targeted BLAST searches, termed FIP-Gre. The search was performed using an amino acid sequence of FIP-Glu (LZ8) from *Ganoderma lucidium* as a query, and the result showed 90% similarity to FIP-Glu. The physiochemical properties are given in (Table 1). Both hydrophilic and hydrophobic amino acids were present in FIP-LZ8 and FIP-Gre. The most prevalent amino acids in FIP-Glu (LZ8) were Asn, Asp, Val, and Thr, whereas the most prevalent amino acids in FIP-Gre were Ala, Asp, Thr, and Val. Both FIPs lack His, Sec, Cys and Pyl amino acids. FIP-Glu (Supplementary Figure 1) as well as FIP-Gre (Supplementary Figure 2) belongs to FIP-Fve domain (PF09259). According to the hydrophilicity prediction results for FIP-Gre, which are shown in Figure 1c, the hydrophilicity is primarily hydrophilic, with an overall average of -0.268, a minimum of -2.38, and a maximum of 1.37.

Table 1: Physiochemical properties of FIP-LZ8 and FIP-Gre computed by ProtParam (Expasy).

No.s	Physiochemical properties	FIP-LZ8	FIP-Gre
1.	Number of amino acids	111	111
2.	Molecular Weight	12509.95Da (12.50kDa)	12458.95Da(12.45KDa)
3.	Isoelectric point PI	4.84	5.14
4.	Instability index (II)	-2.39	1.03
5.	Half-life in mammalian reticulocyte	30 hours	30 hours
6.	Half-life in yeast	>20 hours	>20 hours
7.	Half-life in *E.coli*	>10 hours	>10 hours
8.	Total number of negatively charged residues (Asp + Glu)	12	12
9.	Total number of positively charged residues (Arg + Lys)	10	11
10.	**Formula**	$C_{568}H_{852}N_{146}O_{172}S_1$	$C_{564}H_{855}N_{149}O_{169}S_1$
11.	**Extinction coefficient**	25440	25440
12.	**Aliphatic index**	77.21	81.62
13.	**Grand average of hydropathicity (GRAVY)**	-0.320	-0.268

Multiple Sequence Alignment and Phylogenetic Analysis:

The amino acid sequences of FIPs were retrieved from NCBI (Supplementary Table 2). These sequences were used for sequence alignment by Clustal X (Figure 1a) to analyze sequence homology between them. Protein BLAST from the NCBI revealed that FIPs have a high degree of similarity, between 60% and 90%. FIP- Gre shared 90% homology with the most potent FIP-Glu (LZ8) (P14945.2), 87.39% with FIP-Gca (UOF75531.1), 85.59% with FIP-Gmi (3KCW A), 86.49% with FIP-gat (AJD79556.1) and FIP-Gja (AAX98241.1), 80.56% with FIP-gap (AEP68179.1), 76.85% with FIP-gap2 (ART88472.1), 79.63% with FIP-cru (AKU37620.1), 63.96% with FIP-Fve (P80412.1), 65.14% with FIP-nha (8GO7), 60.19% with FIP-vvo (KAF8653575.1).

The MEGA (version 7.0) phylogenetic tree of FIPs showed that they primarily clustered into five lineages (Figure 1b). The first was the formation of a large distinct lineage by FIP-Gre, FIP-Glu (LZ8), FIP-gat, FIP-Gja, FIP-Gca, and FIP-Gmi. A second lineage was formed by the clustering of FIP-Gca and FIP-Gmi. The third lineage included FIP-cru from *Chroogomphus rutilus* alongside FIP-gap and FIP-gap2, both derived from *Ganoderma applanatum*. There were only two FIPs in the fifth lineage, FIP-nha and FIP-vvo, while FIP-Fve constituted a distinct fourth lineage. FIP-Gre and FIP-Glu appear to be closely related, according to phylogenetic research. Secondary structure prediction indicated that FIP-Gre comprises α-helices, extended β-strands, and random coil, with random coil being most abundant, followed by β-strand and α-helix (Figure 1f). The experimental structure of LZ8 "(Figure 1d) was obtained from the PDB (3F3H), while FIP-Gre models were generated using trRosetta, AlphaFold2, and I-TASSER and evaluated with ERRAT and PROCHECK (SAVES v6.1).

Ramachandran analysis (Supplementary Figure 3(a-c); Supplementary Table 3) showed the AlphaFold2 model (Figure 1e) had the highest stereochemical quality (95.8% residues in most-favored regions; 0% disallowed). Accordingly, the AlphaFold2 model was selected for downstream docking. Structural comparison revealed that FIP-Gre contains four α-helices and sixteen β-sheets and superimposes well with LZ8, consistent with high sequence identity.

Docking Analysis:

The ZDOCK score of top models of docked complexes are presented in (Supplementary Table 4). In view of the effect of both FIPs on EGFR and C-Met, we simulated the binding of FIPs to the EGFR and C-Met by molecular docking. The results showed that FIP-Glu (LZ8) and FIP-Gre interacted with the extracellular segment of EGFR. Interface residues and noncovalent interactions (hydrogen bonds, salt bridges and disulfide proximities) are also detailed in figure 2.

Simulation Results:

Docked complexes were subjected to MD simulations for a timescale of 100ns based on the molecular docking data. The complexes selected for this purpose was those with the highest docking score to observe any alterations in the complex regarding its conformation, stability, and

interactions with amino acid residues throughout the specified time frame. A 100ns molecular dynamics run was subsequently conducted for all complexes. The generated MD trajectories facilitated the evaluation of RMSD, RMSF, and hydrogen bonds of the complexes over time (Figure 3 a-f).

Any changes that occur to the framework of ligand and protein during the simulation are determined by RMSD. Figure 3a shows the RMSD graphs of FIP-Glu and FIP-Gre with EGFR. The overall pattern of RMSD of LZ8-EGFR was similar to FIP-Gre-EGFR in that both of these started to converge to 0.2nm but the RMSD of LZ8-EGFR was higher (0.6-0.8nm) than FIP-Gre-EGFR (0.4nm). The backbone RMSD value of LZ8-EGFR remained nearly stable throughout the 100ns trajectory, with a little deviation at 35ns and 85ns, confirming the stability of the docked complex.

Similarly, the FIP-Gre-EGFR complex was also stable with a little deviation at 85ns. The figure 3b represents that the RMSD backbone of LZ8-C-met is in a same trend that it is superimposed to the RMSD of FIP-Gre-C-met. Both complexes converged between 0.2-0.4nm and remained stable during 100ns trajectory showing the stability of complexes.

To better understand the variations in protein atoms or residues caused by ligand interaction, RMSF analysis was performed for each complex.The RMSF of LZ8 -EGFR show stable trend with slight fluctuations at residue no. 10, 200 and 300 to 0.6nm and the RMSF of FIP-Gre-EGFR was also stable except for residue no. 20 and 250 to a point of 0.6nm (Figure 3c)**.** The RMSF trend of LZ8-C-met was also stable except for the residue no. 100, 200, 550 and 750 raising slightly higher to 0.4nm. The RMSF trend for FIP-Gre-C-met showed slight fluctuations at residue no. 600 and 800 to a point of 0.4nm (figure 3d). All the structures represent low RMSF values around 0.2nm adding to the stability of structures.

In order to further analyze the docked complexes, the hydrogen bonds were observed. Throughout the simulation run (100 ns), hydrogen bond formation was observed, which suggests that the ligand remained in the binding pocket. The number of hydrogen bonds remained high and constant throughout the simulation in the docked complexes including LZ8-EGFR and FIP-Gre-EGFR in figure 3e and a similar trend was followed by LZ8-C-met and FIP-Gre-C-met in figure 3f, showing the stability of protein complexes in docked state.

Gene Synthesis and Coning of Fungal Immunomodulatory Proteins:

Synthetic genes encoding **FIP-Glu (LZ8)**and **FIP-Gre** were codon-optimized for ***E. coli*** and commercially synthesized (Molecular Biology Products, Pakistan). Both genes were cloned into the **pET-29a(+) expression vector** under the **T7 promoter**, with a **C-terminal His_6 tag** to enable Ni-NTA affinity purification. Restriction sites **NdeI (5')**and **XhoI (3')** were introduced for directional cloning. Transformation into *E. coli* **TOP10F'** produced kanamycin-resistant colonies that were **screened by colony PCR** (Supplementary Figure **6c, d)**. Subsequently, the confirmed plasmids **pET-29a(+)-FIP-Glu** and **pET-29a(+)-FIP-Gre** were transformed into *E. coli* **BL21(DE3)**for protein expression. Positive transformants were identified by **colony PCR** using gene-specific primers.

Expression and Purification of Recombinant Proteins

Expression conditions were optimized in BL21 (DE3) cells. Cultures were induced at mid-log phase (OD_{600} = 0.6–0.8) with IPTG at different concentrations (0.2, 0.5, and 1.0 mM) for 16 h at 37 °C. For both FIP-Glu (LZ8) and FIP-Gre, maximal soluble expression was obtained at 0.5 mM IPTG, while induction with 1.0 mM resulted in reduced protein yields (Figure 4a and 4b) respectively. Uninduced controls showed no detectable expression.

Cells were harvested (5,000 × g, 10 min, 4 °C), lysed by sonication in Tris–NaCl lysis buffer containing lysozyme and PMSF, and clarified by centrifugation. The soluble fractions were subjected to Ni-NTA affinity chromatography, resulting in purified proteins of the expected size (~12.5 kDa). Yields were approximately 10 mg/L for FIP-Glu (LZ8) and 6 mg/L for FIP-Gre (Figure 4c, d) respectively. Protein identity was confirmed by Western blotting using anti-His antibodies. Clear bands at ~12.5 kDa were observed for both proteins, while empty-vector controls showed no signal (Figure 4e).

Hemagglutination Assay:

Mouse, human and Sheep red blood cells were used to detect hemagglutination activity of rFIP-Glu and rFIP-Gre. The rFIP-Gre strongly hemagglutinated mouse red blood cells at a minimal concentration of 4µg/mL (Figure 5a) (Supplementary Table 5). Meanwhile rFIP-Glu hemagglutinated mouse red blood cells at a min concentration of 8ug/mL (Figure 5b) (Supplementary Table 6). No hemagglutination activity was observed in human and sheep red blood cells upon adding FIP-Glu and FIP-Gre at concentrations of 0.25 - 128ug/mL.

Anti-bacterial Assay:

Recombinant FIPs, LZ8 and FIP-Gre were tested for their ability to express antimicrobial activity against 5 strains of bacteria including *Staphylococcus aureus, Pseudomonas aeruginosa, E. coli, Salmonella typhi, and Klebsiella pneumoniae*. No zone of inhibition was observed by recombinant LZ8 and FIP-Gre against any of the 5 bacterial strains (Supplementary Figure 4 and 5 respectively). The zones of inhibition were only observed around antibiotic discs used as positive control (Supplementary Table 7 and Table 8). The negative controls containing the Tris-Nacl purification buffer did not show any zones of inhibition.

Cytotoxicity Assay:

Both **rFIP-Glu (LZ8)** and **rFIP-Gre** demonstrated selective cytotoxicity against cancer cell lines (Figure 6), with the most potent activity observed in **A549 cells**, where rFIP-Glu (15.54 µg/mL) was slightly more effective than rFIP-Gre (21.27 µg/mL). Against **HepG2 cells**, both proteins exhibited moderate cytotoxicity, with comparable IC_{50} values (27.59 µg/mL for rFIP-Glu and 29.96 µg/mL for rFIP-Gre). In **MCF-7 cells**, rFIP-Glu showed relatively higher activity (30.38 µg/mL) compared to the weaker effect of rFIP-Gre (43.34 µg/mL). Importantly, neither protein exerted significant toxicity toward the normal **HEK-293** cell line (IC_{50} >100 µg/mL), indicating cancer-selective action.

Anti-cancer Assay:

Morphological Changes:

The morphological observations further supported the cytotoxicity assay results. A549 cells treated with rFIP-Glu (8µg/mL) gradually lost their typical epithelial morphology, with cells becoming rounded, shrunken, and reduced in number compared with the untreated control. Similarly, rFIP-Gre (8µg/mL) treatment caused comparable changes, where cells exhibited loss of adherence, decreased spreading, and visible reduction in density. In contrast, the control group maintained a flattened squamous appearance with clear boundaries and tight adherence to the plate surface (Supplementary Figure 7). These findings confirm that both rFIP-Glu and rFIP-Gre induce cytotoxic effects at the tested concentration, leading to significant alterations in cell morphology and reduced cell viability in A549 cells.

RNA Extraction, Quantification and cDNA Synthesis:

The RNA from control and treated cells with 8µg/ml of rFIPs was extracted and quantified by nanodrop given in the table below (Supplementary Table 9). Later the cDNA was synthesized for treated as well as control groups. The cDNA was confirmed by PCR using GAPDH primers provided with kit and visualized by 1% agarose gel shown in (Supplementary Figure 8).

Gene Expression Studies using qPCR:

qPCR analysis of apoptosis-related genes in A549 cells treated with recombinant FIPs (8 µg/mL) revealed a consistent pro-apoptotic expression pattern. rFIP-Glu (LZ8) upregulated Bax (3.92-fold) and p53 (5.42-fold), alongside significant increases in Caspase 3 (3.44-fold) and Caspase 9 (5.44-fold), while markedly suppressing the anti-apoptotic Bcl-2 (0.45-fold) (Figure 7)

Similarly, rFIP-Gre induced pro-apoptotic shifts, with increases in Bax (2.30-fold), p53 (3.82-fold), Caspase 3 (2.49-fold), and Caspase 9 (3.16-fold), and a reduction in Bcl-2 (0.61-fold) relative to untreated controls. Collectively, these results indicate that both FIP-Glu and FIP-Gre activate the intrinsic mitochondrial apoptosis pathway by enhancing pro-apoptotic and tumor suppressor gene expression while downregulating anti-apoptotic signaling, thereby promoting apoptosis in A549 cancer cells.

Discussion

A novel fungal immunomodulatory protein, **FIP-Gre**, was identified from *Ganoderma resinaceum* through genome mining using LZ-8 (FIP-glu) from *G. lucidum* as a query. Genome mining has proven valuable for characterizing unstudied FIPs, as demonstrated in the identification of FIP-bbo from *Botryobasidium botryosum* [11]. Conserved-domain analysis placed both FIP-Gre and FIP-glu within the **Fve-type family (PF09259)**, which typically encodes 12–13 kDa proteins composed of an N-terminal α-helix and a C-terminal fibronectin type III–like domain. ProtParam profiling predicted hydrophilic character (negative GRAVY) and favorable stability indices, suggesting suitability for soluble expression. Multiple sequence alignment and phylogenetic analysis grouped FIPs into five lineages, with FIP-Gre clustering most closely with LZ-8 and other *Ganoderma* homologs, consistent with earlier reports [11, 25, 26].

The **AlphaFold2** model of FIP-Gre, selected over trRosetta and I-TASSER due to its higher accuracy [27] revealed **four α-helices and sixteen β-strands** that superimpose closely on the crystal structure of LZ-8 (PDB: 3F3H). Model validation using ERRAT, PROCHECK, and Ramachandran analysis confirmed quality, with >95% residues in allowed regions and no disallowed residues, consistent with prior assessments of AlphaFold2 structures [28]. Amino acid composition analysis revealed enrichment of Ala, Asp, Thr, and Val in FIP-Gre, while both FIP-Gre and LZ-8 lacked His and Cys residues, features typical of FIPs [26]. These hydrophilic residues enhance solubility, an important property for recombinant expression and therapeutic applications.

Docking followed by 100-ns molecular dynamics simulations demonstrated stable interactions of FIP-Gre and LZ-8 with EGFR and c-Met, two receptor tyrosine kinases central to cancer progression. Complex stability was supported by low RMSD (0.2–0.4 nm), minimal RMSF fluctuations, and persistent hydrogen bonding, suggesting a ligand-competition mechanism that may interfere with EGF/HGF binding and downstream STAT3/Akt signaling, consistent with other FIPs such as FIP-nha

Integrating in silico and in vitro analyses, FIP-Gre was identified as a novel fungal immunomodulatory protein from *Ganoderma resinaceum* sharing ~90% sequence identity with LZ-8 and adopting a conserved FIP fold consistent with the LZ-8 crystal structure (PDB: 3F3H). Recombinant FIP-Gre expressed from synthetic constructs retained bioactivity in hemagglutination and MTT-based cytotoxicity assays, supporting its potential as an RTK-targeted anticancer candidate [29].

To experimentally validate the computational predictions, in vitro assays were performed in EGFR/c-Met–overexpressing cancer cell lines. Given the low yield and high cost of extracting FIPs from mushroom tissues [30, 31], recombinant expression was prioritized. Previous studies report FIP production at 5–25 mg/L in heterologous systems[32]; therefore, *E. coli* was selected for scalable expression despite known limitations [33].

For cloning and expression, we used the **pET** platform due to the T7 promoter's high output in *E. coli*, convenient N-terminal tag options, a C-terminal His-tag for Ni-NTA purification, and thrombin-cleavable fusion capability [34]. Synthetic **LZ-8** and **FIP-Gre** genes were verified by restriction analysis, amplified in *E. coli* Top10F' for plasmid yield, and subcloned into **pET-29a(+).** Final constructs, **pET-29a(+)-LZ-8** and **pET-29a(+)-FIP-Gre** were transformed into *E. coli* **BL21(DE3)** for induction and purification, enabling the downstream hemagglutination, antimicrobial, MTT, and apoptotic marker assays that characterize their anticancer activity.

For cloning and expression, the pET system was employed due to the strong T7 promoter and compatibility with His-tag–based Ni-NTA purification [35]. Synthetic LZ-8 and FIP-Gre genes were verified by restriction analysis, amplified in *E. coli* Top10F', and subcloned into pET-29a(+). Recombinant constructs were transformed into *E. coli* BL21(DE3) for protein expression and functional evaluation. The workflow followed established protocols for recombinant FIP production using the pET/BL21(DE3) platform [36]. Protein expression was induced with IPTG by relieving LacI repression of the T7 promoter [38]. Optimal soluble expression was achieved at 0.5 mM IPTG, whereas higher concentrations reduced yield, consistent with inducer-associated stress [37]. Purified rLZ-8 and rFIP-Gre migrated at ~12 kDa on SDS-PAGE, and protein identity was confirmed by anti-His Western blotting (Fig. 10), in agreement with previous reports [38].

Functional validation by hemagglutination showed rFIP-Gre to agglutinate mouse RBCs at the lowest tested concentration (4 µg/L, as recorded; Figure 4a), whereas rFIP-Glu required 8 µg/mL (Figure 4b) neither protein agglutinated human or sheep RBCs across 0.25–128 µg/mL, indicating species selectivity at the tested range. Both **rFIP-Gre** and **rFIP-Glu** showed red blood cell specificity, with rFIP-Gre exhibiting stronger hemagglutination at lower concentrations, indicating higher activity toward mouse RBCs. This agrees with [39], who found recombinant LZ-8 expressed in *E. coli* agglutinated mouse but not human or sheep RBCs, whereas *Pichia pastoris* derived LZ-8 displayed broader activity [40]. These results suggest that the **expression host influences FIP structure and receptor specificity**, thereby affecting hemagglutination behavior. Together, these data verify construct integrity, establish induction parameters that favor soluble expression, confirm purity/identity of the recombinant proteins, and demonstrate retained lectin-like activity providing a robust basis for downstream antimicrobial, MTT, and anticancer assays.

Fungal immunomodulatory proteins (FIPs) exert antitumor effects **directly** (e.g., apoptosis, cell-cycle arrest) and **indirectly**via immune activation. Prior work shows rLZ-8 induces apoptosis with G1/S arrest in U-251 MG cells [41], rFIP-gat inhibits growth and triggers G1/S arrest in MDA-MB-231, rFIP-nha and rFIP-ppl display cell type specific cytotoxicity with apoptosis [42]. Consistent with these studies, our MTT assays revealed **selective, cell-type–dependent activity**, highest against **A549** (lung), moderate against **HepG2** (liver), and lower against **MCF-7** (breast), with **no cytotoxicity in HEK293**. This pattern mirrors rFIP-sch3, which showed broad anticancer effects but spared HEK293 [43], supporting FIPs **cancer selectivity** and translational promise. These findings suggested that although FIPs from various sources have sequence conservation, their antitumor efficacy differed significantly.

Following MTT assay results that identified A549 lung cancer cells as the most responsive to treatment, the apoptotic mechanism of fungal immunomodulatory proteins (FIPs) was explored through the expression profiling of Bax, Bcl-2, Caspase-3, Caspase-9, and p53. The concentration of 8µg/mL was selected as it lies near the IC_{50} value, providing sufficient cytotoxic stress to trigger apoptotic pathways while maintaining viable cells for RNA analysis. Morphological alterations like cell shrinkage, rounding, and loss of adherence were evident in treated groups, consistent with hallmark features of apoptosis.

Quantitative RT-PCR analysis revealed significant modulation of apoptosis related genes. Both FIP-LZ8 and FIP-Gre markedly upregulated the pro-apoptotic gene Bax and downregulated the anti-apoptotic gene *Bcl-2*, leading to an increased Bax/Bcl-2 ratio, a well-recognized indicator of mitochondrial pathway activation [44]. Concurrently, p53 expression was elevated, consistent with its role as a transcriptional regulator that

induces Bax and suppresses Bcl-*2* in response to cellular stress and execution of the intrinsic apoptotic cascade [45]. These findings collectively indicate that FIP-induced apoptosis proceeds primarily via the mitochondria dependent pathway.

Our results corroborate earlier studies reporting that FIPs from *Ganoderma* spp. suppress A549 proliferation through G1 arrest and apoptotic signaling [46]. Similar mechanisms have been observed for FIP-gat and FIP-gmi, which trigger cell-cycle arrest and autophagy-mediated cell death through p53 or Akt-mTOR related pathways [47]. The enhanced expression of Bax, Caspase-9, and p53 in our study supports the hypothesis that *Ganoderma* derived FIPs exert their cytotoxicity by activating pro-apoptotic signaling and inhibiting anti-apoptotic regulators.

Together, these findings demonstrate that FIP-Gre and FIP-LZ8 induce apoptosis in lung adenocarcinoma cells through the intrinsic mitochondrial pathway, validating their potential as natural, selective anti-cancer agents. Future investigations integrating protein level validation and in vivo models could further elucidate their therapeutic applicability in targeting EGFR overexpressing tumors.

Conclusion

This study identifies and characterizes FIP-Gre, a novel fungal immunomodulatory protein from *Ganoderma resinaceum*, as a promising anti-cancer agent. In silico analyses revealed its strong structural and functional similarity to LZ-8 and its stable interaction with EGFR and c-Met receptors, while in vitro findings confirmed its selective cytotoxicity against A549 lung cancer cells through apoptosis induction. Together, these results highlight the potential of FIP-Gre as a natural therapeutic candidate for targeted cancer therapy and warrant further preclinical validation.

Abbreviations

Funding: No specific grant from a public, private, or nonprofit organization was obtained for this research.

Conflicts of interest:

The author(s) declared no potential conflicts of interest with respect to the research, authorship, and/or publication of this article.

Acknowledgement:

Dr. Naeem Mahmood Ashraf (School of Biochemistry & Biotechnology, University of the Punjab, Lahore), Higher Education Commission (HEC), Islamabad, Pakistan, University of the Punjab, Lahore and Centre for Applied Molecular Biology (CAMB), University of the Punjab, Lahore

Availability of Data:

The datasets generated and/or analyzed during the current study are not publicly available but are available from the corresponding author on reasonable request.

Declarations

Funding: No specific grant from a public, private, or nonprofit organization was obtained for this research.

Conflicts of interest:

The author(s) declared no potential conflicts of interest with respect to the research, authorship, and/or publication of this article.

Acknowledgement:

Dr. Naeem Mahmood Ashraf (School of Biochemistry & Biotechnology, University of the Punjab, Lahore), Higher Education Commission (HEC), Islamabad, Pakistan, University of the Punjab, Lahore and Centre for Applied Molecular Biology (CAMB), University of the Punjab, Lahore

Availability of Data:

The datasets generated and/or analyzed during the current study are not publicly available but are available from the corresponding author on reasonable request.

References

1. Hsu, H.-C., et al., *Fip-vvo, a new fungal immunomodulatory protein isolated from Volvariella volvacea.* Biochemical Journal, 1997. **323**(2): p. 557-565.

2. Ko, J.-L., et al., *A New Fungal Immunomodulatory Protein, FIP-fve Isolated from the Edible Mushroom, Flammulina velutipes and its Complete Amino Acid Sequence.* European Journal of Biochemistry, 1995. **228**(2): p. 244-249.
3. Uribe-Echeverry, P.T. and G.A. Lopez-Gartner, *Fungal immunomodulatory proteins in the context of biomedicine.* Front. Biosci, 2017. **9**(2): p. 286-306.
4. Liu, Y., S. Bastiaan-Net, and H.J. Wichers, *Current understanding of the structure and function of fungal immunomodulatory proteins.* Frontiers in Nutrition, 2020. **7**: p. 132.
5. Li, S., et al., *FIP-sch2, a new fungal immunomodulatory protein from Stachybotrys chlorohalonata, suppresses proliferation and migration in lung cancer cells.* Applied Microbiology and Biotechnology, 2017. **101**: p. 3227-3235.
6. Ejike, U.C., et al., *New advances and potentials of fungal immunomodulatory proteins for therapeutic purposes.* Critical reviews in biotechnology, 2020. **40**(8): p. 1172-1190.
7. Patel, S.A., et al., *Molecular mechanisms and future implications of VEGF/VEGFR in cancer therapy.* Clinical Cancer Research, 2023. **29**(1): p. 30-39.
8. Bethune, G., et al., *Epidermal growth factor receptor (EGFR) in lung cancer: an overview and update.* Journal of thoracic disease, 2010. **2**(1): p. 48.
9. Ding, P.N., et al., *Risk of Treatment-Related Toxicities from EGFR Tyrosine Kinase Inhibitors: A Meta-analysis of Clinical Trials of Gefitinib, Erlotinib, and Afatinib in Advanced EGFR-Mutated Non-Small Cell Lung Cancer.* J Thorac Oncol, 2017. **12**(4): p. 633-643.
10. Carvalho, B., et al., *The role of c-Met and VEGFR2 in glioblastoma resistance to bevacizumab.* Scientific reports, 2021. **11**(1): p. 6067.
11. Wang, Y., et al., *Identification of a Novel Anti-cancer Protein, FIP-bbo, from Botryobasidium botryosum and Protein Structure Analysis using Molecular Dynamic Simulation.* Sci Rep, 2019. **9**(1): p. 019-42104.
12. Gasteiger, E., et al., *Protein identification and analysis tools on the ExPASy server*. 2005: Springer.
13. Wang, Y., et al., *Protein domain identification methods and online resources.* Comput Struct Biotechnol J, 2021. **19**: p. 1145-1153.
14. Felsenstein, J., *Confidence limits on phylogenies: an approach using the bootstrap.* evolution, 1985. **39**(4): p. 783-791.
15. Zhou, S., et al., *Molecular cloning, codon-optimized gene expression, and bioactivity assessment of two novel fungal immunomodulatory proteins from Ganoderma applanatum in Pichia.* Applied Microbiology and Biotechnology, 2018. **102**(13): p. 5483-5494.
16. Laskowski, R.A., et al., *PROCHECK: a program to check the stereochemical quality of protein structures.* Journal of applied crystallography, 1993. **26**(2): p. 283-291.
17. Chen, R., L. Li, and Z. Weng, *ZDOCK: an initial-stage protein-docking algorithm.* Proteins: Structure, Function, and Bioinformatics, 2003. **52**(1): p. 80-87.
18. Laskowski, R.A., et al., *PDBsum: Structural summaries of PDB entries.* Protein science, 2018. **27**(1): p. 129-134.
19. DeLano, W.L., *The PyMOL molecular graphics system.* http://www. pymol. org/, 2002.
20. Olaleye, M. and C. Bello-Michael, *Comparative antimicrobial activities of Aloe vera gel and leaf.* African journal of biotechnology, 2005. **4**(12).
21. Morten, B.C., R.J. Scott, and K.A. Avery-Kiejda, *Comparison of three different methods for determining cell proliferation in breast cancer cell lines.* Journal of visualized experiments: JoVE, 2016(115).
22. Fulkerson, H.L., et al., *Overview of human cytomegalovirus pathogenesis.* Human Cytomegaloviruses: Methods and Protocols, 2021: p. 1-18.
23. Rehman, S., et al., *Antiviral activity of Acacia nilotica against Hepatitis C Virus in liver infected cells.* Virology Journal, 2011. **8**(1): p. 220.
24. Rio, D.C., et al., *Purification of RNA using TRIzol (TRI reagent).* Cold Spring Harbor Protocols, 2010. **2010**(6): p. pdb. prot5439.
25. Qu, Z.W., et al., *Recombinant Expression and Bioactivity Comparison of Four Typical Fungal Immunomodulatory Proteins from Three Main Ganoderma Species.* BMC Biotechnol, 2018. **18**(1): p. 018-0488.
26. Ramlal, A. and A. Samanta, *In Silico functional and phylogenetic analyses of fungal immunomodulatory proteins of some edible mushrooms.* AMB Express, 2022. **12**(1): p. 022-01503.
27. Jumper, J., et al., *Highly accurate protein structure prediction with AlphaFold.* Nature, 2021. **596**(7873): p. 583-589.
28. Binbay, F.A., et al., *Quality Assessment of Selected Protein Structures Derived from Homology Modeling and AlphaFold.* Pharmaceuticals, 2023. **16**(12).
29. Wu, J.R., et al., *Preclinical trials for prevention of tumor progression of hepatocellular carcinoma by LZ-8 targeting c-Met dependent and independent pathways.* PLoS One, 2015. **10**(1).
30. Ko, J.L., et al., *A new fungal immunomodulatory protein, FIP-fve isolated from the edible mushroom, Flammulina velutipes and its complete amino acid sequence.* European Journal of Biochemistry, 1995. **228**(2): p. 244-249.

31. Lin, J.w., et al., *Gene cloning of a novel fungal immunomodulatory protein from Chroogomphis rutilus and its expression in Pichia pastoris.* Journal of Chemical Technology & Biotechnology, 2016. **91**(11): p. 2761-2768.
32. Yeh, C.M., et al., *Extracellular expression of a functional recombinant Ganoderma lucidium immunomodulatory protein by Bacillus subtilis and Lactococcus lactis.* Applied and environmental microbiology, 2008. **74**(4): p. 1039-1049.
33. Idalia, V.-M.N. and F. Bernardo, *Escherichia coli as a model organism and its application in biotechnology.* Recent Adv. Physiol. Pathog. Biotechnol. Appl. Tech Open Rij. Croat, 2017. **13**: p. 253-274.
34. Mierendorf, R.C., et al., *Expression and Purification of Recombinant Proteins Using the pET System.* Methods Mol Med, 1998. **13**: p. 257-92.
35. Li, S., et al., *Recombinant expression of a novel fungal immunomodulatory protein with human tumor cell antiproliferative activity from Nectria haematococca.* Int J Mol Sci, 2014. **15**(10): p. 17751-64.
36. Li, F., et al., *Gene cloning and recombinant expression of a novel fungal immunomodulatory protein from Trametes versicolor.* Protein Expr Purif, 2012. **82**(2): p. 339-44.
37. Liu, Z.Q. and P.C. Yang, *Construction of pET-32 α (+) Vector for Protein Expression and Purification.* N Am J Med Sci, 2012. **4**(12): p. 651-5.
38. Wu, G., et al., *Identification and Functional Characterization of a Novel Immunomodulatory Protein From Morchella conica SH.* Front Immunol, 2020. **11**(559770).
39. Xue, Q., et al., *Functional expression of LZ-8, a fungal immunomodulatory protein from Ganoderma lucidium in Pichia pastoris.* J Gen Appl Microbiol, 2008. **54**(6): p. 393-8.
40. Bastiaan-Net, S., et al., *Biochemical and functional characterization of recombinant fungal immunomodulatory proteins (rFIPs).* International Immunopharmacology, 2013. **15**(1): p. 167-175.
41. Cong, W.R., et al., *Production and functional characterization of a novel fungal immunomodulatory protein FIP-SN15 shuffled from two genes of Ganoderma species.* Appl Microbiol Biotechnol, 2014. **98**(13): p. 5967-75.
42. Li, S.Y., et al., *Identification and functional characterization of a novel fungal immunomodulatory protein from Postia placenta.* Food Chem Toxicol, 2015. **78**: p. 64-70.
43. Li, S., et al., *Identification and Characterisation of a Novel Protein FIP-sch3 from Stachybotrys chartarum.* PLoS One, 2016. **11**(12).
44. Gao, C. and A.Y. Wang, *Significance of increased apoptosis and Bax expression in human small intestinal adenocarcinoma.* J Histochem Cytochem, 2009. **57**(12): p. 1139-48.
45. Brentnall, M., et al., *Caspase-9, caspase-3 and caspase-7 have distinct roles during intrinsic apoptosis.* BMC Cell Biology, 2013. **14**(1): p. 32.
46. Wu, C.T., et al., *Ling Zhi-8 mediates p53-dependent growth arrest of lung cancer cells proliferation via the ribosomal protein S7-MDM2-p53 pathway.* Carcinogenesis, 2011. **32**(12): p. 1890-6.
47. Chiu, L.Y., et al., *Immunomodulatory Protein from Ganoderma microsporum Induces Pro-Death Autophagy through Akt-mTOR-p70S6K Pathway Inhibition in Multidrug Resistant Lung Cancer Cells.* PLoS One, 2015. **10**(5).

Figures

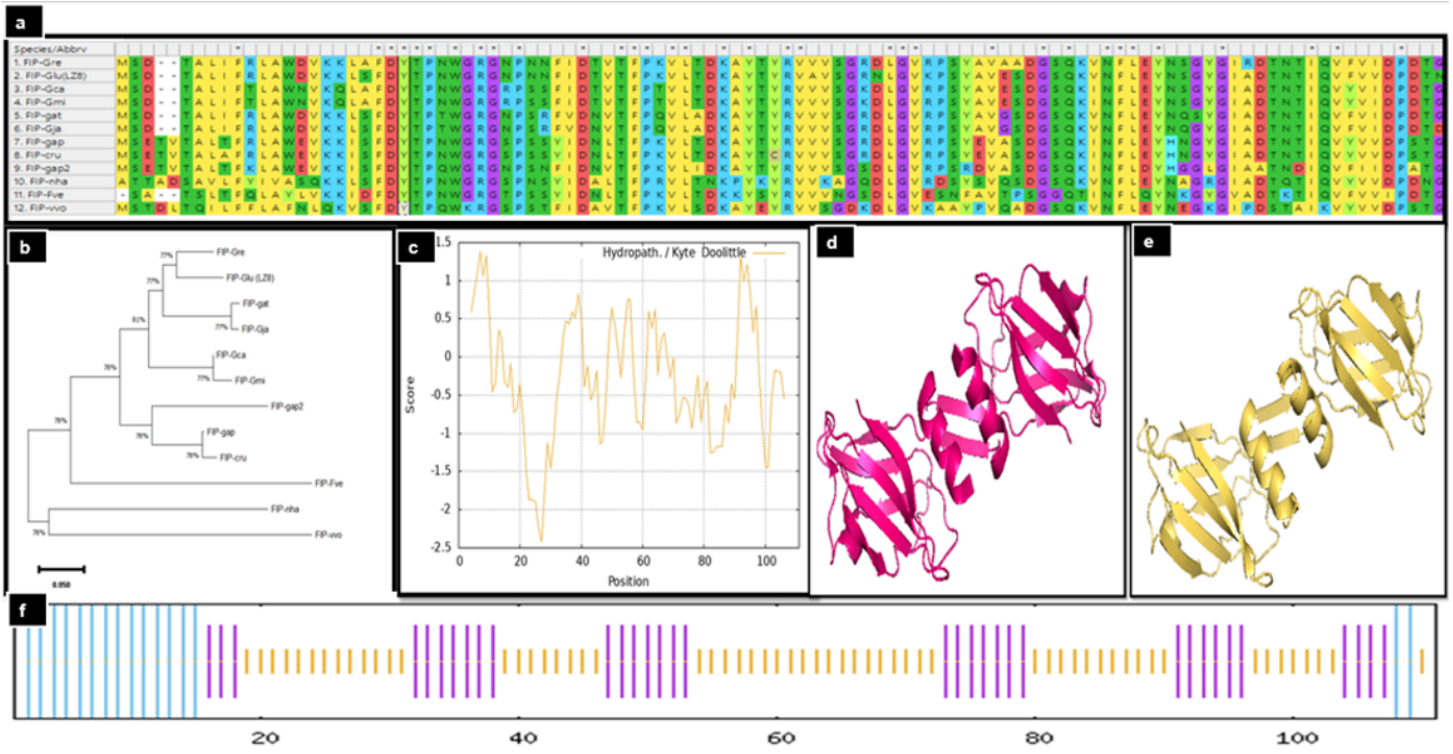

Figure 1

Amino acid sequence alignment, phylogenetic analysis and Structure prediction of FIP-Gre. (a)Sequence Alignment of FIP-Gre with selected known FIPs where similar amino acids are represented by same color and the amino acid identities are marked by asterisks. (b)Phylogenetic tree of FIPs constructed by MEGA software (version 7.0) using the neighbour-joining method. (c) hydropathicity profile indicating a predominantly hydrophilic character. (d) 3D model of LZ8 retrieved from PDB. (e) predicted 3D model of FIP-Gre generated by AlphaFold2 (f) secondary structure prediction showing α-helices (blue), extended β-strands (purple) and random coils (orange).

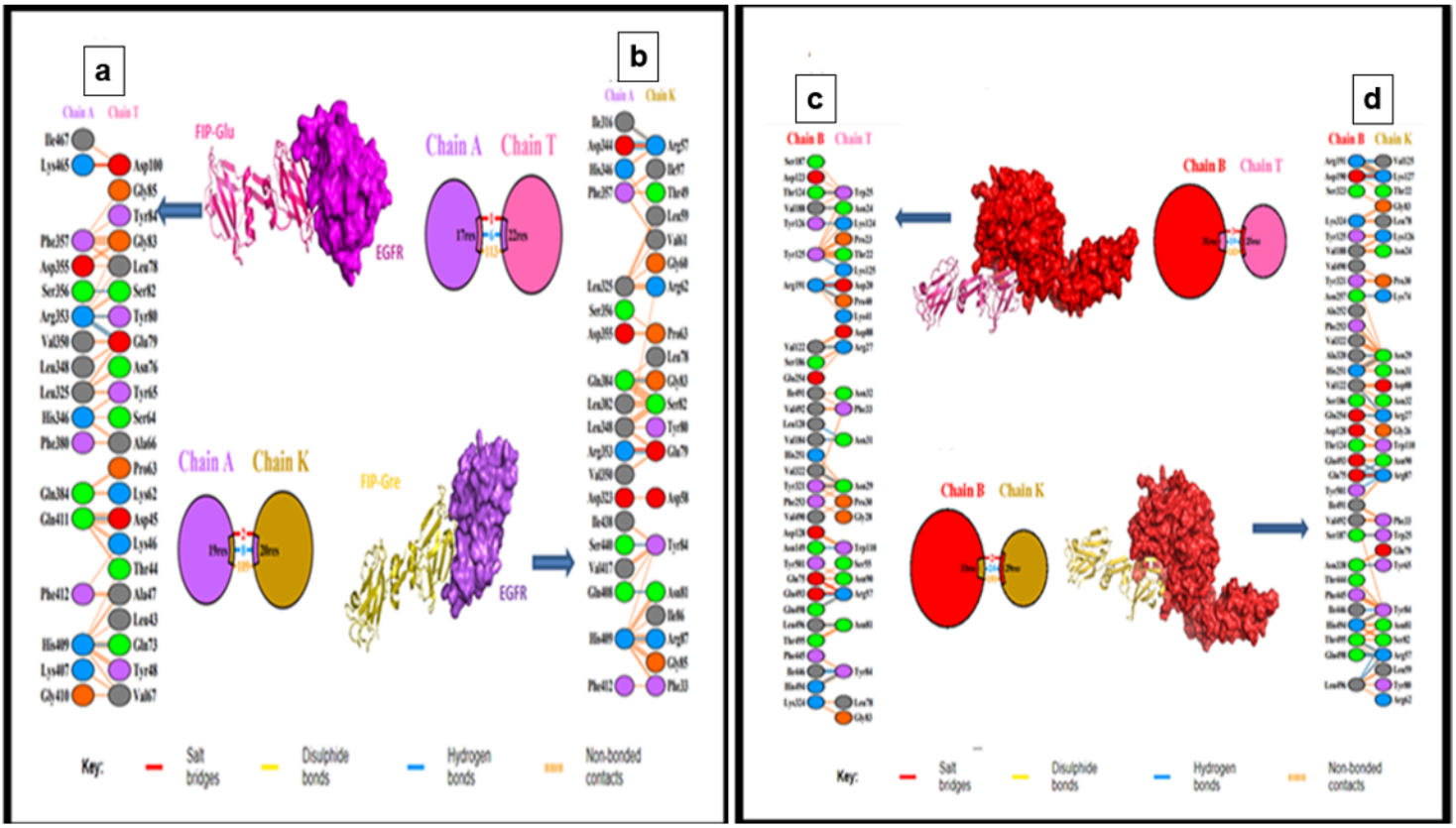

Figure 2

ZDOCK Server generated docked complex (a) Interaction residues showing H- bonds, salt bridges and Disulphide bonds between chain A (EGFR) and chain T (FIP-Glu). (b) Interaction residues showing H- bonds, salt bridges and Disulphide bonds between chain A (EGFR) and chain T (FIP-Gre). (c) Interaction residues showing H- bonds, salt bridges and Disulphide bonds between chain B (c-met) and chain T (FIP-Glu). (d) Interaction residues showing H- bonds, salt bridges and Disulphide bonds between chain B (c-met) and chain K(FIP-Gre).

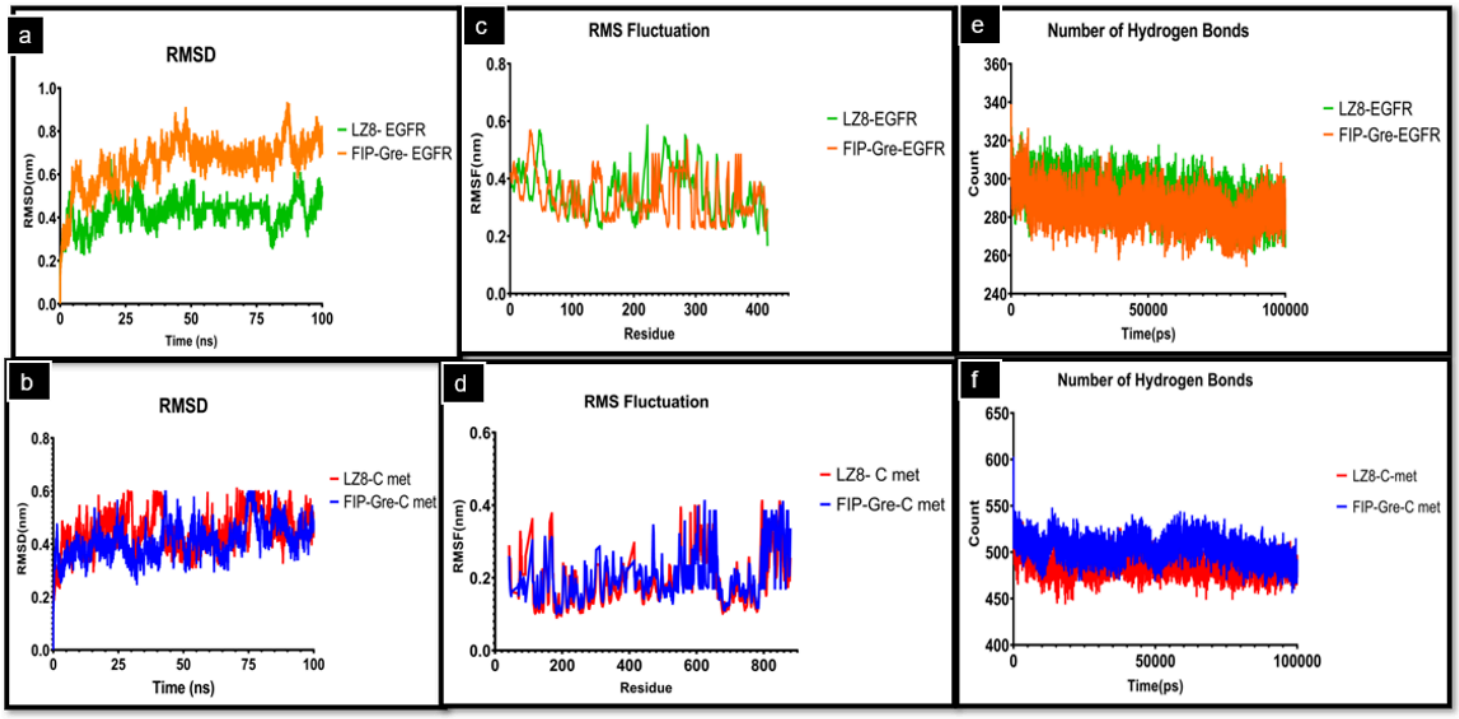

Figure 3

Molecular Simulation result analysis (a) RMSD graph of docked complexes of LZ8 and FIP-Gre with EGFR. (b) RMSD graph of docked complexes of FIP-Glu and FIP-Gre with C-met. The abscissa is time (ns) and the ordinate is RMSD (nm). The orange, green, red and blue colors are for LZ8-EGFR, FIP-Gre-EGFR, LZ8-C-met and FIP-Gre-C-met respectively. (c) RMSF graph of docked complexes of FIP-Glu and FIP-Gre with EGFR. (d) RMSF graph of docked complexes of FIP-Glu and FIP-Gre with C-met. The abscissa is time (ns) and the ordinate is RMSF (nm). The orange, green, red and blue colors are for LZ8-EGFR, FIP-Gre-EGFR, LZ8-C-met and FIP-Gre-C-met respectively. (e) The graph showing the hydrogen bond count of protein complexes of FIP-Glu and FIP-Gre with EGFR. (f) The graph showing the hydrogen bond count of protein complexes of FIP-Glu and FIP-Gre with C-met. The abscissa is time (ps) and the ordinate is the number of hydrogen bonds in complexes. The orange, green, red and blue colors are for LZ8-EGFR, FIP-Gre-EGFR, LZ8-C-met and FIP-Gre-C-met respectively. The abscissa is time (ps) and the ordinate is the number of hydrogen bonds in complexes. The orange, green, red and blue colors are for LZ8-EGFR, FIP-Gre-EGFR, LZ8-C-met and FIP-Gre-C-met respectively.

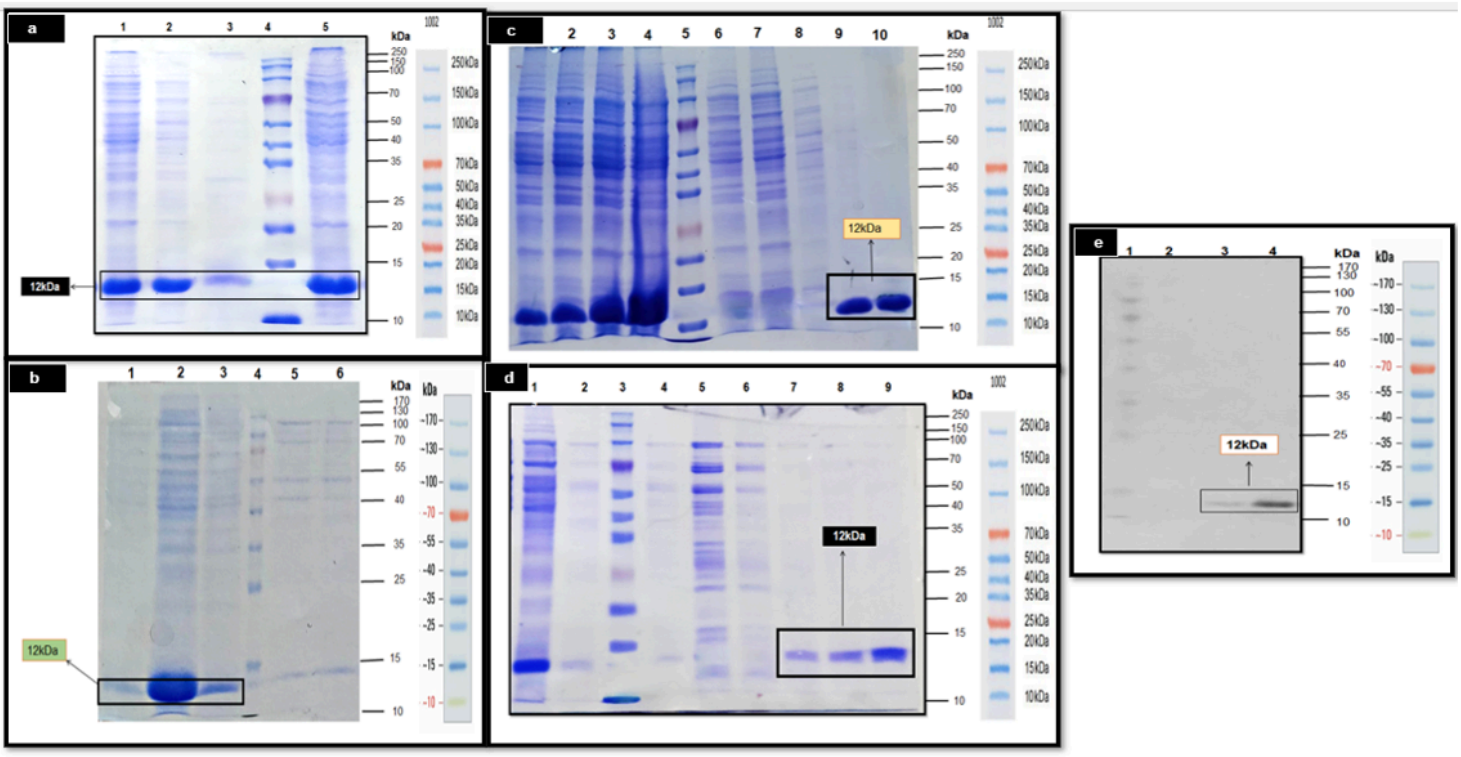

Figure 4

Effect of IPTG induction and purification of recombinant proteins. (a) SDS-PAGE analysis of rFIP-Glu (LZ8) expression at different IPTG concentrations (0.2, 0.5, and 1.0 mM) compared with uninduced control. Lane 1 induced sample of BL21 (DE3) lysate containing pET29a (+)-LZ8 with 0.2mM IPTG. Lane 2 induced sample of BL21 (DE3) lysate containing pET29a (+)-LZ8 with 1mM IPTG. Lane 3 uninduced sample of BL21 (DE23) lysate containing pET29a (+)-LZ8 (without IPTG induction). Lane 4 prestained ladder Prestained Protein Ladder, 10 to 180 kDa (Thermo). Lane 5 induced sample of BL21 (DE3) lysate containing pET29a (+)-LZ8 with 0.5mM IPTG. (b) SDS-PAGE analysis of rFIP-Gre expression under the same IPTG induction conditions. Lane 1 induced sample of BL21 (DE3) lysate containing pET29a (+)-FIP-Gre with 1mM IPTG. Lane 2 induced sample of BL21 (DE23) lysate containing pET29a (+)-FIP-Gre with 0.5mM IPTG. Lane 3 induced sample of BL21 (DE3) lysate containing pET29a (+)-FIP-Gre with 0.2mM IPTG. Lane 4 prestained ladder Prestained Protein Ladder, 10 to 180 kDa (Thermo). Lane 5&6 uninduced sample of BL21 (DE3) lysate containing pET29a (+)-FIP-Gre (without IPTG induction). (c) SDS PAGE of rFIP-LZ8, Lane 1-4, Total protein sample, lane 5 Prestained protein marker (ZOKEYO HPR1002; lane 6 & 7, Protein Flow through, lane 8, wash, lane 9 & 10, purified rLZ8. (d) SDS PAGE of FIP-Gre, Lane 1, Total protein sample, lane 2, 4 & 6, Wash. Lane 3, Prestained protein marker (ZOKEYO HPR1002; lane 5, Protein Flow through, lane 7,8 & 9, purified rFIP-Gre. (e) Western blot analysis of rFIPs. Lane 1, Prestained Protein Ladder, 10 to 180 kDa, 26616 (Thermo). Lane 2, empty vector. Lane 3, Purified rLZ8. Lane 4, purified FIP-Gre.

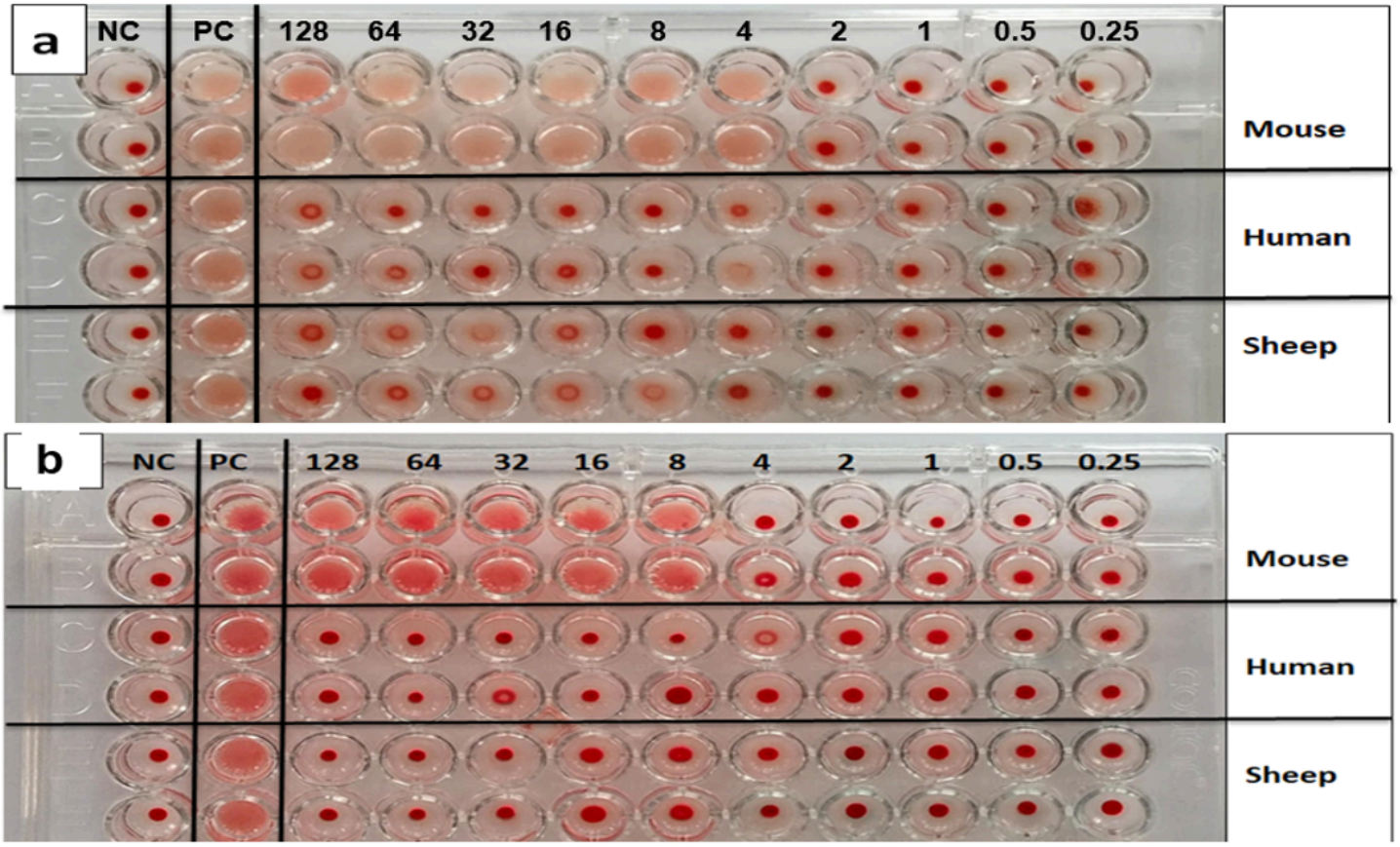

Figure 5

The hemeagglutination assay of rFIPs. (a) The hemagglutinating ability of rFIP-Gre at different concentrations (128, 64, 32, 16, 8, 4, 2, 1, 0.5, 0.25µg/ml) from well 3-12, towards red blood cells of Mouse, human and sheep. PHA (2 µg/ml) was used as a positive control to assess the basic response generated under our conditions of experimentation (well 2). 1XPBS was used a negative control. (b) The hemagglutinating ability of rLZ8 at different concentrations (128, 64, 32, 16, 8, 4, 2, 1, 0.5, 0.25µg/ml) from well 3-12, towards red blood cells of Mouse, human, sheep as well as rabbit. PHA (2 µg/ml was used as a positive control to assess the basic response generated under our conditions of experimentation (well 2). 1XPBS was used a negative control.

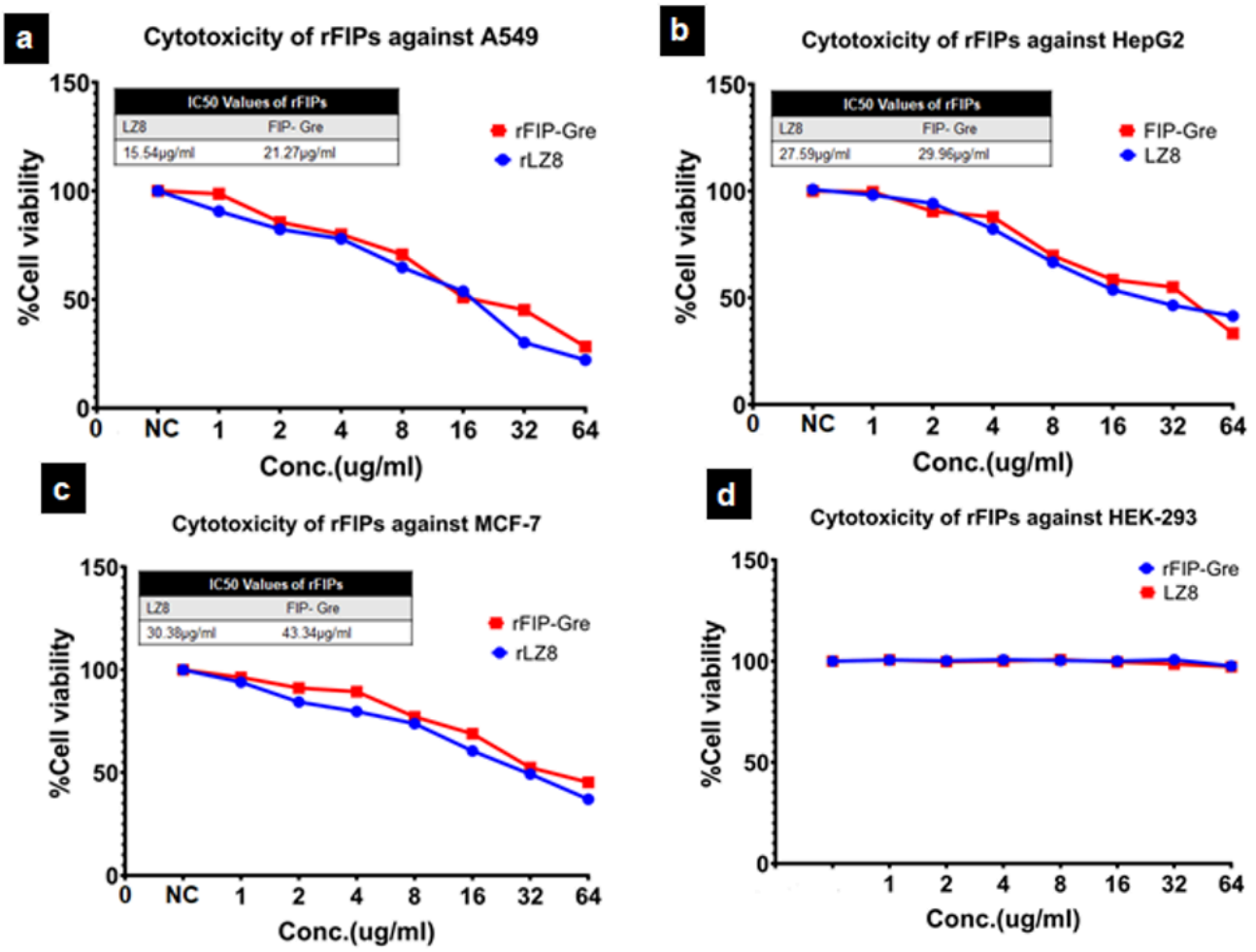

Figure 6

Cytotoxic effects of recombinant FIPs against cancer and normal cell lines.Dose–response curves from MTT assay showing the effect of rFIP-Glu (LZ8) and rFIP-Gre on (a) A549 lung adenocarcinoma cells, (b) HepG2 hepatocellular carcinoma cells, (c) MCF-7 breast cancer cells, and (d) HEK-293 normal human embryonic kidney cells. IC_{50} values (µg/mL) were calculated using nonlinear regression in GraphPad Prism 8.0.

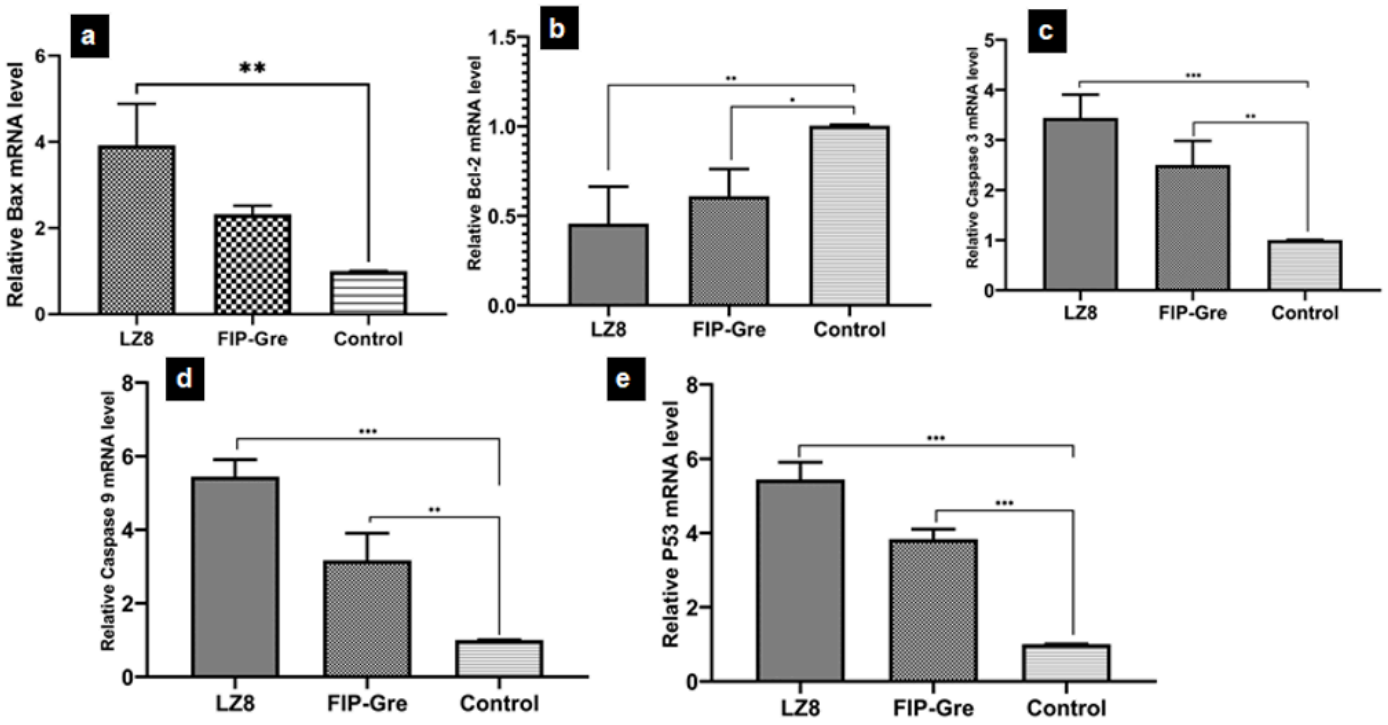

Figure 7

Relative mRNA expression of apoptosis-related genes in A549 cells treated with recombinant FIPs (8 µg/mL). Quantitative PCR analysis showing fold changes in (a) Bax, (b) Bcl-2, (c) Caspase 3, (d) Caspase 9, and (e) p53 expression following treatment with rFIP-Glu (LZ8) and rFIP-Gre compared with untreated controls. Data are presented as mean ± SD (n = 3). Statistical significance was determined by one-way ANOVA (*p < 0.05, **p < 0.01, ***p < 0.001).

Supplementary Files

This is a list of supplementary files associated with this preprint. Click to download.

- SupplementaryData.docx